Stability of Second Generation HTS Pancake Coils at 4.2 K for High Heat Flux Applications

C. L. H. Thieme, K. J. Gagnon, J. Y. Coulter, H. Song, and J. Schwartz, *Fellow, IEEE*

***Abstract*—We explored high magnetic field superconducting properties and stability at 4.2 K of Second Generation High Temperature Superconductors using both short conductors and small pancake coils. Short lengths of conductor were tested at 4.2 K and 0–25 T in parallel and perpendicular fields, demonstrating an overall critical current of 420 A/mm^2 in a parallel field of 25 T. A 56 m length of wire was carefully characterized for performance along the length in self-field at 77 K, and in 10 m lengths at 75 K and a 0.52 T field oriented parallel and perpendicular to the face of the conductor. These characterized lengths were made into small pancake coils which were equipped with a central heater, voltage taps and taps for thermocouples. We report on the stability testing at 4.2 K of one of these coils.**

***Index Terms*—High magnetic fields, high-temperature superconductors, stability, superconducting coils.**

I. Introduction

A SIGNIFICANT issue in future superconducting magnet technology for colliders is an increasing irradiation dosage that deposits heat while damaging the conductor and other magnet materials [1], [2]. Interest in high temperature superconductors (HTS) arises from the anticipated large energy margin due to the high transition temperature and very high upper critical field of the HTS materials, which is much higher than that of $\mathrm{Nb_3Sn}$.

In the manufacture of Second Generation High Temperature Superconductor (2G HTS) YBCO wire, the process used by American Superconductor (AMSC) provides the flexibility to engineer 2G performance, architectures and stabilizer materials towards a variety of applications [4]–[6]. These so-called "344 superconductors" are produced using the RABiTS/MOD approach [7]. They are also of interest for High Energy Physics applications as the critical current at high fields can be substantial [8], [9]. The manufacturing technology is based on the coating of wide bi-axially textured foils, which offers a significant cost advantage over other technologies. Second, the stabilization of the 344 superconductors is achieved with a lamination process. The laminate material can be selected to have a low or high electrical and thermal conductivity and it allows great flexibility in adapting the 344 superconductors to the desired application. In this project, we looked at the stability of 344 superconductors laminated with a copper stabilizer, occupying 50% of the cross-section.

Characterizations of short lengths of early 2G HTS wires demonstrated a potential for high performance at 25 T and 4.2 K, showing an engineering critical current of 200 $\mathrm{A/mm^2}$ [8]. For actual applications, this number is on the low side as insulation needs to be added. A doubling of this performance to 400 $\mathrm{A/mm^2}$ in a conductor with 50% copper stabilizer makes the superconductor more attractive for high field use. More recent process improvements have increased performance at higher temperatures. At 4.2 K as well, a high performance was demonstrated in short lengths of R&D type 344 superconductors at fields of up to 15 T [9]. In this work we used well-characterized longer lengths of high performance 344 superconductors to measure high field performance at 4.2 K. We use the same wires for stability measurements in a background field of 6 T.

II. Coil Manufacture and Characterization

A. Manufacture of 344 Superconductors

The manufacture of 2G HTS wires is based on a thin film approach. The active component, the YBCO $(\mathrm{YBa_2Cu_3O_7})$ or (RE)BCO layer, is $\sim 1\ \mu\mathrm{m}$ thick, but despite the fact that only one such layer is present in a single conductor, $\mathrm{J_e}$ can reach over 130 $\mathrm{A/mm^2}$ at 77 K, self-field (SF). This high performance requires well-aligned YBCO grains with very low grain boundary mis-orientation angles. Templates for growing these near-single crystal-like YBCO films are therefore very well-textured. AMSC uses a bi-axially textured NiW substrate onto which thin epitaxial oxide buffer layers are deposited (RABiTS). The YBCO layer is grown using a low-cost, solution-based Metal Organic Deposition (MOD) process. The process is also amenable to chemical modifications and doping to improve flux pinning and enhance in-field performance. The coating process is presently done on a 40 mm wide foil.

After YBCO reaction and Ag coating, the conductor is slit to 4 mm. This slit "insert" wire is laminated on both sides to a slightly wider copper foil (4.4 mm), see example in Fig. 1. The superconductor for this Phase I Project was made using an

Manuscript received August 25, 2008. First published June 23, 2009; current version published July 15, 2009. This work was supported in part by the US Department of Energy.

C. L. H. Thieme is with the American Superconductor, Devens, MA 01434 USA (e-mail: cthieme@amsc.com).

K. J. Gagnon was with the American Superconductor. He is now at the Chemistry Department, Texas A&M University, College Station, Texas 77843 USA (e-mail: kgagnon@mail.chem.tamu.edu).

J. Y. Coulter is with the Superconductivity Technology Center, Los Alamos National Laboratory, Los Alamos, NM 87545 USA (e-mail: jycoulter@lanl.gov).

H. Song is with the National High Magnetic Field Laboratory, Florida State University, Tallahassee, FL 32310 USA (e-mail: hsong@magnet.fsu.edu).

J. Schwartz is with the Department of Mechanical Engineering and National High Magnetic Field Laboratory Florida State University, Tallahassee, FL 32310 USA (e-mail: schwartz@magnet.fsu.edu).

Color versions of one or more of the figures in this paper are available online at http://ieeexplore.ieee.org.

Digital Object Identifier 10.1109/TASC.2009.2017914

Fig. 1. Cross section of 4.4 mm wide 344 superconductors. Top and bottom are 0.05 mm copper stabilizers. Center section contains the buffered NiW substrate with YBCO coating.

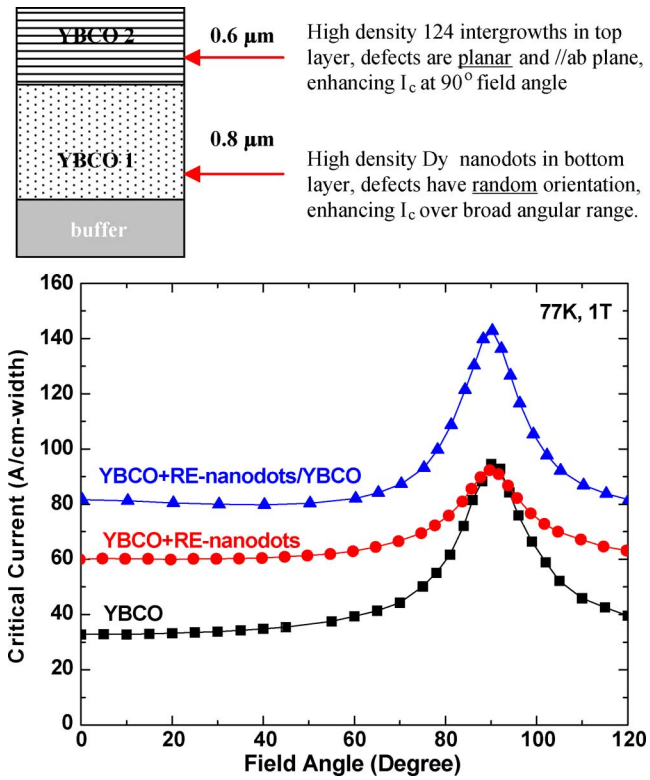

Fig. 2. Sketch of double YBCO architecture (top) and field-angle dependence of I_c (bottom). Bottom curve: 0.8 μm thick YBCO layer, no doping. Mid curve: 0.8 μm thick YBCO layer with RE doping. Top curve: 0.8 μm thick YBCO layer with RE doping + 0.6 μm thick YBCO layer with planar defects, giving a 1.4 μm thick hybrid YBCO layer.

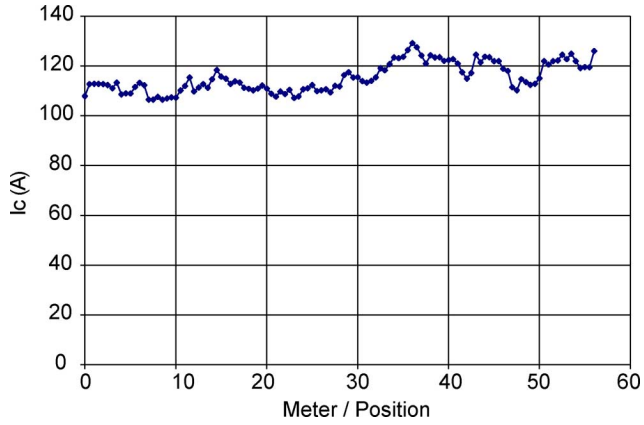

Fig. 3. I_c along the length of a 56 m long section of 344 superconductors, 0.5 m voltage tap distance, 77 K, SF.

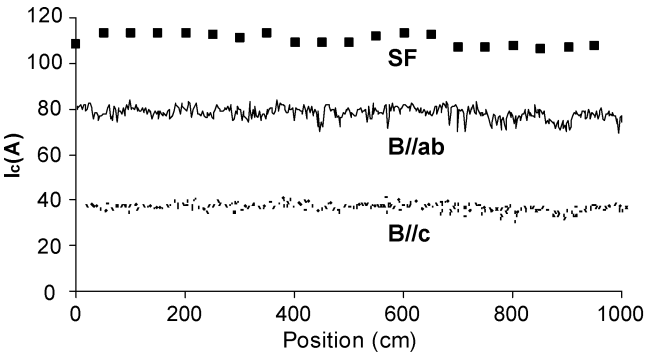

Fig. 4. I_c (75.5 K) along 10 m length, B = 0.52 T, in parallel (B//ab) and perpendicular (B//c) orientation. Y. Coulter, LANL.

experimental double coat technology for the YBCO layer. The double coat has a total thickness of 1.4 μm, comprised of two layers which are chemically different and formulated to give the desired flux pinning properties. For example, for undoped YBCO the difference between parallel and perpendicular field direction is high at all temperatures. R&D flux pinning efforts are therefore geared towards retention of the high J_c in the parallel field orientation while enhancing J_c in the perpendicular field orientation.

An example is shown in Fig. 2 [6], where precipitates called nanodots enhance the perpendicular-field I_c values in the first coat. Planar 124 stacking faults (top layer) maintain effective ab-plane pinning in the second coat. Other than this double-coat technology, production and testing followed standard AMSC manufacturing procedures and methods.

B. Characterization at 77 K

56 m of 344 superconductors were tested at 77 K, SF, using a $1\mu\mathrm{V/cm}$ criterion and a 1 m tap distance, in a continuous manner. Data are taken every 0.5 m. Fig. 3 shows the I_c results along this 56 m length. Minimum I_c is 106 A, while the maximum I_c is 130 A. For the pancake coil manufacture, we used 10 m lengths starting at 0 m. Short lengths which were used for the high field measurements were taken from the 45–56 m position. A detailed knowledge of I_c variability along the length is of importance when the stability results are interpreted. Low I_c variability is essential in ensuring that quenching will initiate near the heating element and not in sections with a low local I_c. For this reason two of the 10 m lengths were also measured at LANL continuously.

The LANL facility measures I_c on a much shorter length scale, and uses a small background field. Measurements of the 10 m lengths were done at 75.5 K and a background field of 0.52 T, which could be rotated in a perpendicular or parallel field orientation; tap distance was 2 cm. In Fig. 4 the top curve (squares) is the original measurement at AMSC at zero field. The continuous curves are the I_c values for a parallel (top, B//ab) and perpendicular field (bottom, B//c).

The ratio at 0.52 T is ~2. A second 10 m length, not shown, had comparable results. Statistics of both lengths are shown in Table I. Standard deviations varied between 3.5 to 5.3%.

C. Manufacture of Small Pancake Coils

The 344 superconductors for the manufacture of the small pancake coils were helically wrapped with paper insulation. 10 m lengths were used per coil, which had a 50 mm ID, an 81 mm OD, and 48 turns. In the middle of the coil a heater strip was inserted, consisting of a thin (0.025 mm) Inconel foil, carefully cut to a 2 mm width with four evenly spaced

TABLE I
STATISTICS IN TWO 10 m LONG 344 SUPERCONDUCTORS, 0.52 T (Y. COULTER, LANL)

I_c statistics	First 10 m length		Second 10 m length	
Field orientation	B//ab	B//c	B//ab	B//c
I_c – max (A)	84.2	41.5	91.8	46.4
I_c – min (A)	69.5	30.0	66.8	31.8
I_c – mean (A)	78.2	37.0	83.9	41.9
I_c – St dev (A)	2.7	1.8	3.5	2.2
I_c – St dev (%)	3.5	4.9	4.2	5.3

Fig. 5. Small pancake coil using first length of 10 m of 344 superconductors (see Table I), with current leads and voltage taps (wide and narrow Cu foils) and centrally located heater, one full turn, for stability testing in liquid He.

taps for contact to a power supply. The heater was electrically well-insulated from the conductor. The heater extended over one full turn. Voltage taps were distributed on either side of the heater, and in a radial direction as well. Also included were small copper taps to attach thermocouples rather than inserting the thermo-couples between layers during winding. These taps work well for cryo-cooler mounted coils; for submerging in a liquid cryogen the taps need to be thermally insulated with a small amount of foam.

Coils were tested as wound, after epoxy-impregnation, and after several thermal cycles, before stability testing at FSU. One of the coils is shown in Fig. 5. Current leads were widened at the base to create a large current injection area, needed for the 400–800 A anticipated for testing at 4.2 K. The final V-I curve after potting and thermal cycling is shown in Fig. 6. I_c is 77 A at 77 K, SF, and 0.1 $\mu V/cm$. The 25% reduction in I_c compared to the continuous I_c wire tests is due to the perpendicular field components at 77 K which will reduce I_c in the inner windings. This effect is much less at lower temperatures and in a background field, when coil I_c and short sample test results are expected to agree well. The transition is sharp, with an index value $n = 31$ $(V \sim (I/Ic)^n)$.

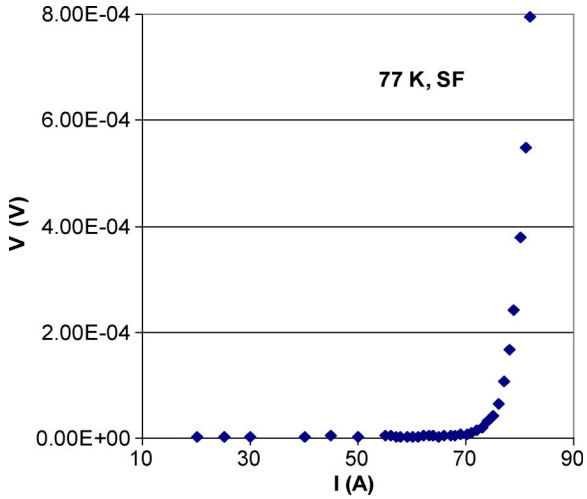

Fig. 6. 77 K V-I curve for pancake coil at 77 K. Index value $n = 31$ $(V \sim (I/Ic)^n)$.

D. Characterization at 4.2 K

Short samples measuring 120 A at 77 K, SF, were tested at 4.2 K and fields of 0–25 T, at the NHMFL. For parallel fields a modified ITER-type probe was used, suitable for a tape-like geometry. Four voltage taps were used, with a 40 or 60 cm tap distance. Like the ITER probe for testing Nb_3Sn wire, this probe aimed at having the entire conductor length between the voltage taps at the same field.

Current injection length was around 20 cm. Current direction was selected such that the sample would be in compressive hoop stress in field. A rig for short U-shaped samples was used for the $B_{//c}$ orientation.

Both measurements were carried out in a standard 52 mm bore, 25 T Bitter magnet at the NHMFL. Fig. 7 shows I_c versus $B_{//c}$. Fig. 8 shows I_c versus $B_{//ab}$. I_c in a perpendicular field $B_{//c}$ is about a factor of 5–6 lower than I_c in a parallel field $B_{//ab}$. For 2G HTS coils (solenoids or racetrack) operating in a parallel background field, the results in parallel field (Fig. 8) are the most relevant. Note that with the 0.96 mm^2 conductor cross section, I_c (A) and J_e (A/mm^2) are numerically virtually the same. At 25 T in parallel field, the engineering critical current is around 420 A/mm^2.

Strain sensitivity of this double coat conductor was re-measured at 77 K, and was no different from the standard conductor with a 0.8 μm YBCO layer. We do not anticipate significant changes in the strain dependence at 4.2 K and high magnetic fields, which was earlier measured at both 50 K and 4.2 K, using a Walter Spring [10]. At 4.2 K and 19 T and at 0.45% strain, I_c was reduced by about 14%, but this reduction was completely reversible.

When loaded up to 0.55% strain, I_c was irreversibly reduced to about 95% of its original value. 0.4% appears a safe strain limit at high magnetic fields.

The angular dependence of this wire was determined at 7 T, and is shown in Fig. 9. Even at a relatively low field of 7 T the increased ratio $I_c(B//ab)/I_c(B/c/)$ to >4 compared to a ratio of 2 at 77 K is evident.

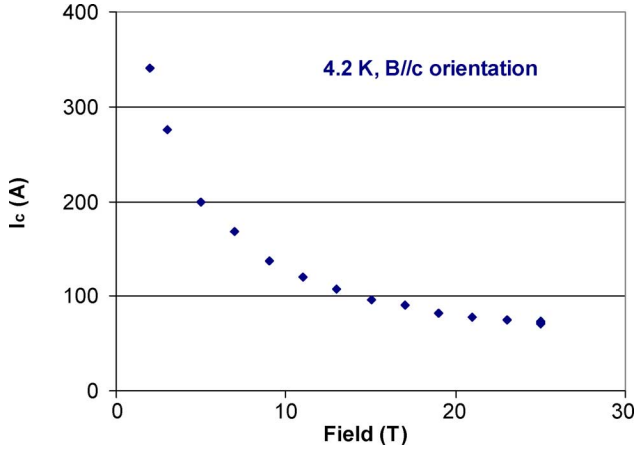

Fig. 7. Short sample I_c versus perpendicular magnetic field $B_{//c}$ at 4.2 K. 1 cm tap distance, 1 $\mu V/cm$ criterion. Cross sectional area (50% Cu) is 0.96 mm^2.

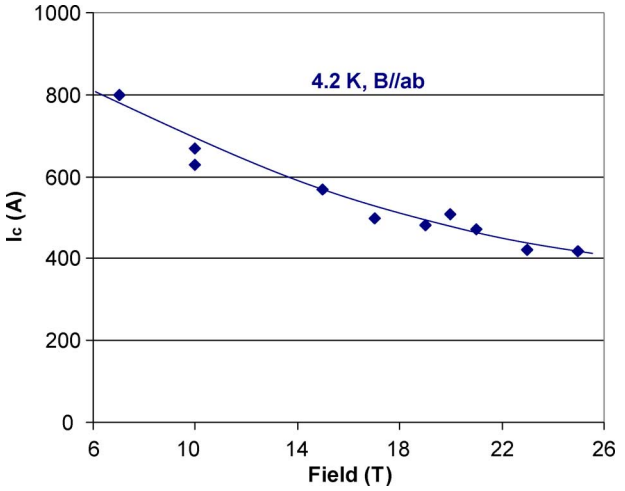

Fig. 8. I_c versus parallel magnetic field $B_{//ab}$ at 4.2 K, 1 m long sample, 40 cm tap distance, 0.1 $\mu V/cm$ criterion. Cross sectional area is 0.96 mm^2, including the 50% copper section. At 25 T the engineering critical current is 420 A/mm^2.

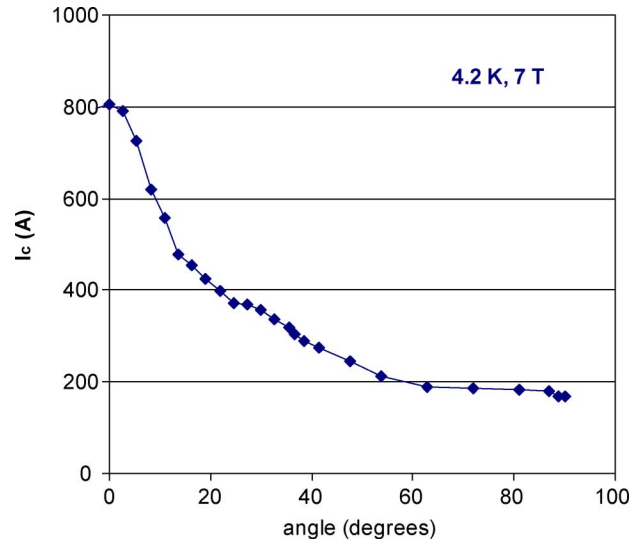

Fig. 9. I_c versus field angle at 4.2 K and 7 T.

III. Coil Stability Testing

A. Stability Testing Approach

Stability testing of the coil shown in Fig. 6 was performed in a 6 T background magnetic field provided by a 200 mm warm bore, cryocooled superconducting magnet. The resulting peak hoop stress on the conductor in the coil is 0.31 MPa per Ampere of transport current. To ensure that the steady-state hoop stress during stability testing remained well below the conductor stress limit, the transport current was limited to 500 A, corresponding to a hoop stress of 155 MPa. Note that this does not take into account local stresses within the conductor due to quenching. The magnitude and effects of these transient stresses remain unknown in YBCO coated conductors and depend in part upon the normal zone propagation velocity. Thus, in order to minimize the likelihood of damage to the coil, the steady-state operating stress was kept to a conservatively low level.

To prepare for in-field stability testing, the coil was mounted to a G10 plate using black Stycast 2850 FT. The G10 was cut with the lamination in radial direction. The current leads were laminated with Bi2223 conductors to decrease the Joule heating. The coil and leads were then reinforced using white Stycast 1266 and fiber glass. After centering the coil, the coil assembly was tightly screwed onto the main G10 board beneath the measurement probe. At this point, the remaining instrumentation wiring was attached and the helium sensor position was adjusted to ensure that the helium level would be kept at least 25 cm above the coil upper surface. The probe was then inserted into the cryostat within the magnet. The background field was slowly ramped to 6 T, after which the YBCO coil was cooled slowly down to liquid helium. The entire cool-down process from room temperature to 4.2 K required about 8.6 hours.

Stability testing ensued via two approaches. In the first set of tests, the ability of the coil to remain stable during current ramping and while maintaining a steady-state transport current for an extended period was tested. In all cases, the coil was ramped at 1 A/s. In the second set of tests, a steady-state heat load was applied while the transport current was maintained at an otherwise stable steady-state value. Due to a malfunction temperature was not recorded during these runs. Voltage at various locations in the coil was used to detect changes in stability.

B. Stability Test Results

Fig. 10 shows the series of test results for the first set of stability experiments. In Fig. 10(a), $I(t)$ and $E(t)$ are shown for the coil first being ramped to 100 A, held steady for about 15 minutes, and then ramped to 200 A and held for 7 minutes. A non-zero electric field $\sim 0.5\ \mu V/cm$ was observed during both ramp steps. The coil remained stable at both $I = 100$ A and $I = 200$ A. One electric field spike occurred at about $t = 21$ minutes which may be a flux jump. At $t \sim 26$ minutes the coil current was ramped down to zero. Fig. 10(b) shows $I(t)$ and $E(t)$ for the second testing of the coil. In this case, the coil was step-ramped to 200 A, held for about 20 minutes, ramped in two steps to 300 A and held for 7 minutes. Again, $E \sim 0.5\ \mu V/cm$ was observed during ramping. A few flux jumps were again seen at 200 A and at 300 A.

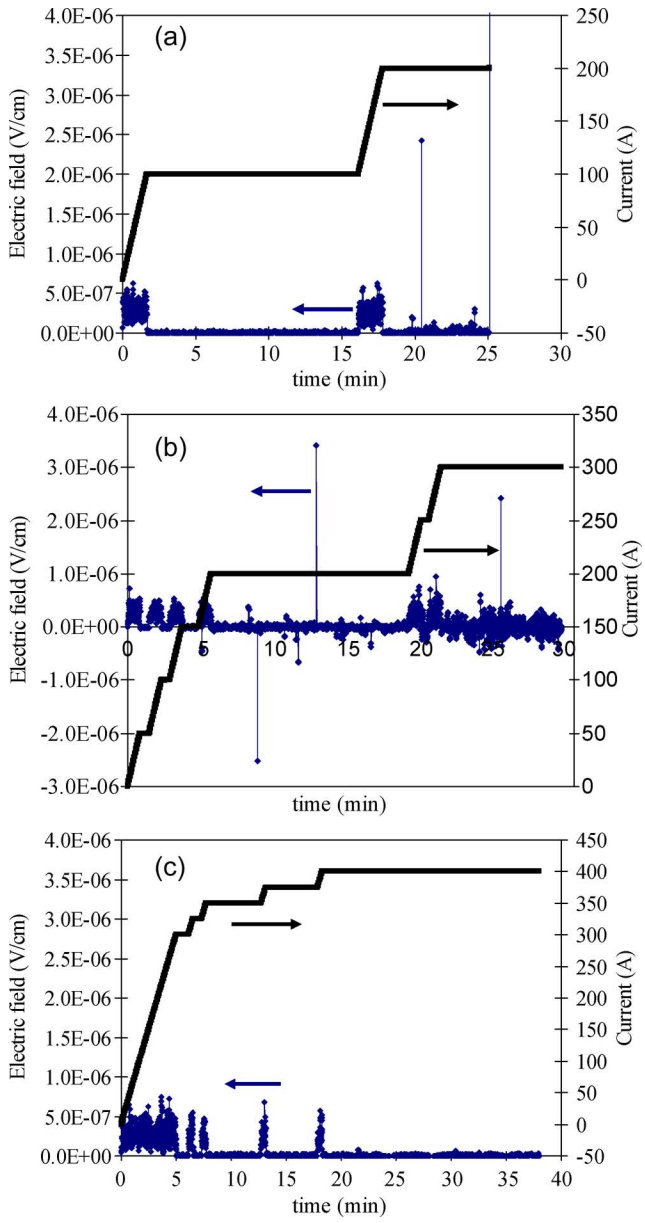

Fig. 10. $E(t)$ and $I(t)$ for studying the coil stability during ramping and steady-state transport current, at 4.2 K and a background field of 6 T. (a), (b) and (c) curves represent three sequential tests of the coil, each going to higher current (200, 300 and 400 A).

Despite the few flux jumps, the coil was stable. Lastly, as seen in Fig. 10(c), the coil was ramped directly to 300 A and then step-ramped to 400 A where it was held for 20 minutes. During the ramping to 300 A, $\mathrm{E} \sim 0.5\ \mu\mathrm{V/cm}$ but with a number of spikes to about $\mathrm{E} \sim 0.7\ \mu\mathrm{V/cm}$ which may be flux jumps. During the subsequent step-ramp, the typical $\mathrm{E} \sim 0.5\ \mu\mathrm{V/cm}$ was observed. No flux jumps were observed for $\mathrm{I} > 300$ A, including the 20 minute hold at 400 A (unless these flux jumps produced much lower electric field than those seen at lower current). The coil was stable at 400 A.

The second set of stability testing, which uses the heater embedded within the coil, began with $I = 400$ A. The initial heat load was 0.01 $\mathrm{W/cm^2}$ which was held for 1 minute while monitoring the coil voltage. If no voltage rise was seen in the coil, then the heat load was increased by 0.01 $\mathrm{W/cm^2}$ and held steady for another minute.

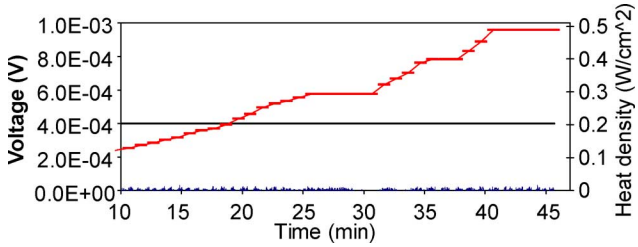

Fig. 11. $V(t)$ and $heat(t)$ for studying coil stability with steady-state $I = 400$ A and a progressively increasing heat load.

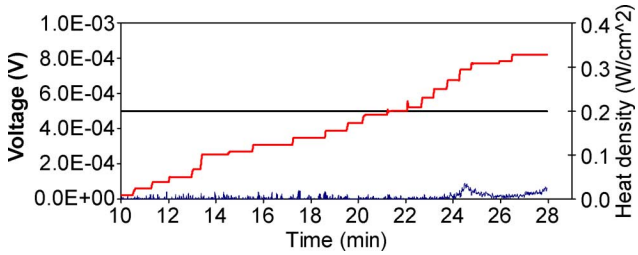

Fig. 12. $V(t)$ and $heat(t)$ for studying coil stability with steady-state $I = 500$ A and a progressively increasing heat load. The first indication of quenching is seen at $heat = 0.294$ W/cm2.

This process was repeated until the heat load reached $0.30\mathrm{W/cm^2}$, at which point the heat load was held for 5 minutes. No voltage increase was observed, so the heat was increased in 0.01 $\mathrm{W/cm^2}$ increments (1 minute each) until reaching 0.40 $\mathrm{W/cm^2}$ which was held for 3 minutes, and then to 0.5 $\mathrm{W/cm^2}$ which was held for 5 minutes. The 0.5 $\mathrm{W/cm^2}$ corresponds to a total heat dissipation of 3.2 W in the one-turn heater. $V(t)$ and the heat load ramping are seen in Fig. 11. The non-zero voltage in the first 10 minutes, due to ramping the coil to 400 A, is not shown.

There were no subsequent voltage spikes (flux-jumps) or systematic increases due to the heat load. The coil was stable. In the last coil stability experiment, the current was ramped to 500 A. In this case, the initial steady-state heat load was again 0.01 $\mathrm{W/cm^2}$ and this was increased in a step-and-hold manner similar to the experiment at 400 A. The $V(t)$ and the heat load ramping for this case are seen in Fig. 12. The voltage was tracked at various locations in the coil, and the end-to-end voltage could directly be related to the voltage generated near the heater turn. In the run of Fig. 12 the heat load was increased to 0.294 $\mathrm{W/cm^2}$, the voltage rose to 0.08 mV and then returned to zero, indicating a disturbance and recovery. The voltage began to increase again for a heat load of 0.328 $\mathrm{W/cm^2}$, at which point the experiment was terminated to prevent damage to the coil. At this point the 0.328 $\mathrm{W/cm^2}$ corresponds to a total heat dissipation of 2.2 W in the one-turn heater.

IV. Discussion

A. J_e (4.2 K, B)

Earlier $\mathrm{J_c}$ (4.2 K, B) measurements at FNAL using short sections of 344 superconductors with high $\mathrm{I_c}$ [9] showed an increasing ratio of $\mathrm{I_c(B_{//ab})/I_c(B_{//c})}$ with increasing field, from

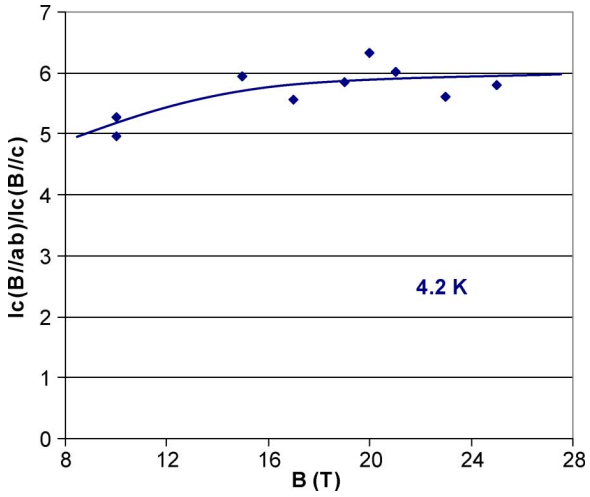

Fig. 13. $I_c(B_{//ab})/I_c(B_{//c})$ ratio versus magnetic field B at 4.2 K..

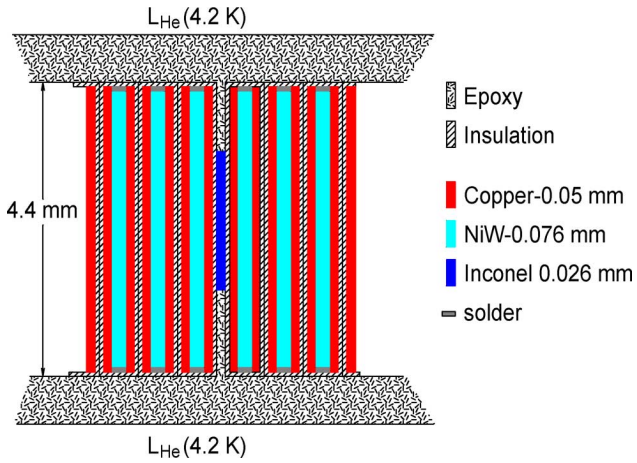

Fig. 14. Sketch of cross section of coil in vicinity of centrally located heater (Inconel). The epoxy thickness was 0.6 mm at the bottom and 1.6 mm at the top.

2–3 at 1 T to around 7 at 14 T. This ratio, unlike Bi-2223, was nearly temperature independent from 4.2 K to 33 K. In the present wire with a slightly lower I_c the ratio tends to saturate at around 6 at fields above 15 T and at 4.2 K, as can be seen in Fig. 13. The high 7:1 ratio in the earlier work might have been related to I_c difference between wire pieces used for the perpendicular and parallel field measurements. The I_c values at 77 K, for the parallel field orientation, were within a few percent for earlier and present work (127 and 120 A, respectively). At 4.2 K and field the earlier wire had a 15% higher I_c, suggesting that the earlier samples probably had a higher degree of planar pinning. The 6:1 ratio is high for applications in which both perpendicular and parallel field components are experienced. For regular solenoids, for example, a 2:1 ratio is believed to be acceptable.

For the present purpose in which the 344 superconductors would be used in a parallel background field generated by a LTS-based magnet, a 6:1 ratio is disadvantage but not prohibitive. Insert coils generating 5–6 T in a background field of 20 T will see the influence of a 2–3 T perpendicular component, which will reduce the overall J_e somewhat.

B. Stability Considerations

An interpretation of the stability measurements from Fig. 11 and Fig. 12 is difficult due to the absence of good temperature data close to the heater. We therefore used the following approach.

First, we calculated the ideal case in which the coil remains superconducting up to the temperature when I_c reaches 400 and 500 A. For this we made an estimate of the field experienced by the superconductor near the heater and then used earlier I_c (B,T) data for the same type of wire [9].

Second, we estimated the local temperature using thermal modeling (3D ANSYS) of the coil section around the centrally located heater. A sketch of the heater environment is shown in Fig. 14; the 2 mm wide heater is located at mid height. The heater extended over one full turn, positioned in the geometric middle of the coil. For the thermal modeling we used in-house measurements of the thermal conductivity in coils stacks of 344 superconductors in two directions. The first direction was parallel to the conductor. The second direction was perpendicular to the face of the conductor, across a number of insulating layers. Heat capacity was measured as a function of temperature by Quantum Design. For power dissipation we used the final total dissipated power at 400 and 500 A.

Third, we compared these two temperatures: the transition temperature and the anticipated final temperature from the steady state heating. At 400 and 500 A currents the magnetic field in the coil can be calculated as function of location. Near the inner turns, the field is highest, and its orientation is mainly parallel to that of the applied field.

At 400 and 500 A DC the self-fields in that location are 0.93 and 1.16 T, respectively, and the 400 A and 500 A levels therefore correspond to 50 and 63% of short sample I_c at 6.93 and 7.13 T, respectively.

The self-field is low near the center of the heater (mid-plane of the coil) but then rapidly increases towards the top and bottom of the coil. Fig. 15 shows the combined field strength which would be seen by the superconductors next to the heater. It ranges form 0.33 in the center to 0.83 T near the edge of the heater, and neighboring superconductor. We assumed the average to be 0.6 T to calculate the expected I_c (B)-T plot. At 6.6 T (the background field combined with the self-field) we do not have any direct measurements but can deduce J_c (6.6 T)-T from earlier data as measured by FNAL [9]. For this, their I_c (B,T) values have been scaled down by 15%, and the results are shown in Fig. 16. From Fig. 16 we can determine the anticipated transition temperatures at 400 and 500 A.

These can now be compared with the final steady state temperatures predicted by the thermal modeling study, for the two total dissipation levels of 2.2 and 3.2 W experienced at the end of the runs shown in Figs. 11 and 12. Table II shows the comparison.

For the 400 A case (50% of I_c) the thermal modeling predicts a slightly higher temperature (+1.4 K) than the transition temperature expected from Fig. 6. For the 500 A case (63% of I_c) the thermal modeling predicts a slightly lower temperature (−1 K) than this transition temperature. In both cases there is a discrepancy (no transition at 400 A and the onset of a transition at

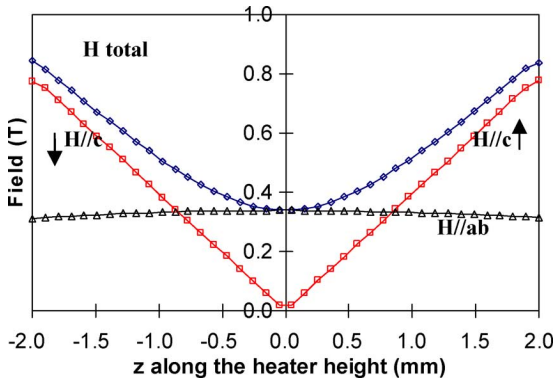

Fig. 15. Self-field of coil near heater, from top to bottom of coil (along the 4 mm width of the neighboring 344 superconductors).

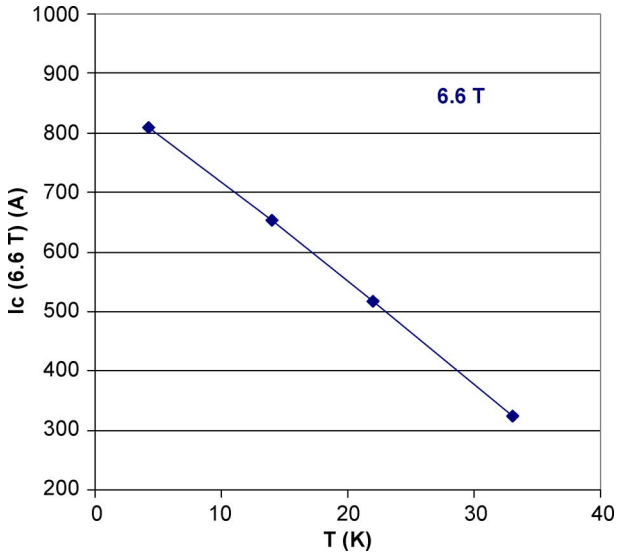

Fig. 16. $I_{c(6.6\ T)}$ versus temperature. Values have been calculated using data from a similar 344 superconductor, measured at FNAL [9].

TABLE II
TRANSITION TEMPERATURES TCS AT 6.6 T (Fig. 16) AND FINAL TEMPERATURE FROM HEATER INPUT, THERMAL MODELING

I_{OP}	T_{CS} – FIG. 16	T –THERMAL MODEL
400 A (50% I_c)	28.7 K	30.1 K
500 A (62% I_c)	23.0 K	22.0 K

500 A). However, in both cases a significant thermal margin is predicted for a coil operating at 4.2 K, at 50–63% of I_c, in a field of ~7 T. This thermal margin is not limited to this relatively low field: even at 15 T the predicted transition temperatures would be 22 K and 17 K for an operating current of 50 and 62% of I_c, respectively, for a coil operating at 4.2 K.

V. CONCLUSIONS

From a critical current density perspective, Second Generation High Temperature Superconductors can be successfully used at 4.2 K and in parallel background fields of 10–25 T. In short samples we demonstrated an overall (engineering) critical current of 420 A/mm^2 at 25 T ($B_{//ab}$) in 344 superconductors with 50% copper. The $I_c(B_{//ab})/I_c(B_{//c})$ ratio saturated to around 6 at 25 T. Thermal stability at 4.2 K and high magnetic fields also shows significant potential for 344 superconductors. We characterized several 10 m lengths at 75.5 K and in a 0.52 T background field and established a relatively high I_c homogeneity along the length. We tested a small pancake coil made with this wire which was provided with a centrally located heater. The coil could be run in a stable manner at 4.2 K and a background field of 6 T. At a current of 400 A (50% of I_c) the temperature was approximately 29-30 K near the heater. At 500 A (63% of I_c) a voltage onset was observed at a temperature of 22–23 K near the heater.

ACKNOWLEDGMENT

The authors would like to thank J. Yuan, AMSC, for his thermal modeling studies, P. Yankauskas, AMSC, for coil winding, Y. Coulter, LANL, for his continuous I_c measurements, and U. Trociewitz, NHMFL, for assistance with the coil measurements.

REFERENCES

[1] A. Devred, S. A. Gourlay, and A. Yamamoto, "Future accelerator magnet needs," *IEEE Trans. Appl. Supercond.*, vol. 15, no. 2, pp. 1192–1199, 2005.

[2] N. K. Mokhov, D. R. Chichili, S. A. Gourlay, S. Van Sciver, and A. Zeller, "Superconducting magnets in high-radiation environment at supercolliders," presented at the Super Magnets for Supercolliders Workshop, Erice, Sicily, Oct. 2003, FERMILAB-Conf-06-244-AD, Jul. 2006, unpublished.

[3] R. Gupta, M. Anerella, M. Harrison, J. Schmalzle, and A. Zeller, "Radiation-resistant HTS quadrupole for RIA," *IEEE Trans. Appl. Supercond.*, vol. 15, no. 2, pp. 1149–1152, 2005.

[4] X. Li, M. W. Rupich, C. L. H. Thieme, M. Teplitsky, D. Buczek, E. Siegal, D. Tucker, J. Schreiber, K. DeMoranville, J. Inch, R. Savoy, and S. Fleshler, this conference.

[5] A. P. Malozemoff, S. Fleshler, M. Rupich, C. Thieme, X. Li, W. Zhang, A. Otto, J. Maguire, D. Folts, J. Yuan, H.-P. Kraemer, W. Schmidt, M. Wohlfart, and H.-W. Neumueller, "Progress in high temperature superconductor coated conductors and their applications," *Supercond. Sci. Technol.*, vol. 23, p. 034005, 2008.

[6] S. Fleshler, A. P. Malozemoff, and M. Rupich, "Scale up of 2G wire manufacturing at American superconductor," in *Supercond. for Electric Syst. 2007 Annu. Peer Rev.* [Online]. Available: http://www.energetics.com/supercon07/agenda.html

[7] A. Goyal, D. P. Norton, J. D. Budai, M. Paranthaman, E. D. Specht, D. M. Kroeger, D. K. Christen, Q. He, B. Saffian, F. A. List, D. F. Lee, P. M. Martin, C. E. Klabunde, E. Hardtfield, and V. K. Sikka, *Appl. Phys. Lett.*, vol. 69, p. 1975, 1996.

[8] M. W. Rupich, U. Schoop, C. Thieme, D. T. Verebelyi, W. Zhang, X. Li, T. Kodenkandath, N. Nguyen, E. Siegal, L. Civale, T. Holesinger, A. Goyal, and M. Paranthaman, "Second generation HTS wire based on RABiTS substrates and MOD YBCO," *IEEE Trans. Appl. Supercond.*, vol. 15, p. 2458, 2005.

[9] D. Turroni, E. Barzi, M. Lamm, V. Lombardo, C. Thieme, and A. V. Zlobin, "Angular measurements of HTS critical current for high field solenoids," *Adv. Cryog. Eng.: Trans. ICMC*, no. 54, pp. 451–458, 2008.

[10] D. Uglietti, B. Seeber, V. Abacherli, W. L. Carter, and R. Flukiger, "Critical currents versus applied strain for industrial Y-123 coated conductors at various temperatures and magnetic fields up to 19 T," *Supercond. Sci. Technol.*, vol. 19, pp. 869–872, 2006.